CHEMICAL ENGINEERING TRANSACTIONS

VOL. 72, 2019

A publication of AIDIC

The Italian Association of Chemical Engineering
Online at www.aidic.it/cet

Guest Editors: Jeng Shiun Lim, Azizul Azri Mustaffa, Nur Nabila Abdul Hamid, Jiří Jaromír Klemeš

ISBN 978-88-95608-69-3; **ISSN** 2283-9216

DOI: 10.3303/CET1972001

Removal of β-naphthol in Water via Photocatalytic Degradation over N-TiO_2/SiO_2 Nanocomposite under Simulated Solar Light Irradiation

Duy Thao Nguyen, Thi Ngoc Suong Ho, Minh Vien Le*

Faculty of Chemical Engineering, Ho Chi Minh city University of Technology, 268 Ly Thuong Kiet, 14 Ward, District 10, Ho Chi Minh City, Vietnam
lmvien@hcmut.edu.vn

In the present study, photocatalytic materials of TiO_2/SiO_2 and nitrogen-dopedTiO_2/SiO_2 were prepared by sol–gel method. Their photocatalytic activities were evaluated using β-naphthol solution with a 25 W lamp (Natural light PT 2191-ExoTerra) as the simulated solar light source. Physico-chemical properties of photocatalytic materials were characterised by X-ray diffraction (XRD), energy dispersive X-ray (EDX), N_2 adsorption–desorption isotherms and ultraviolet-visible diffuse reflectance spectroscopy. The effects of the nitrogen (N) content and calcination temperature on the morphology and photocatalytic activity of TiO_2/SiO_2 were investigated. A Visible-light response was obtained with N-doped TiO_2/SiO_2 materials, resulting in high degradation of β-naphthol (10 ppm) from 89.41 % to 95.4 %, which was higher than that of P25 (58.75 %).

1. Introduction

β-naphthol, one of the naphthalene derivatives, is the most important industrial chemicals and used extensively in dyestuffs manufacturing, pharmaceutical production and biogeochemical processes (Ma et al., 2017). This compound is usually present in drinking water and industrial wastewater while being quite slowly and incompletely biodegradable. Those techniques which have been carried out to remove or eliminate β-naphthol in water such as biological, membranes, evaporation have some limitations (Qu et al., 2013), because of secondary environmental pollution.

In the past decade, semiconductor photocatalysis has been recognised as an efficient strategy for the degradation of environmental pollutants into friendly products or less harmful ones (Vaiano et al., 2016b). Titanium dioxide, TiO_2, is considered a potential of photocatalyst for the degradation of organic pollutant in aqueous medium due to its non-toxicity (Vaiano et al., 2016b), relatively low cost (Makhdoomi et al 2015), high chemical stability (Vaiano et al., 2017,) and superior photocatalytic activity (Kumar et al., 2017). The large bandgap of TiO_2 causes little absorption of visible light (Hu et al., 2017), resulting in very low quantum yield in light to energy conversion. These have limited the practical utilisation of this material. To consume sunlight in the photocatalytic process of TiO_2 efficiently, it is necessary to narrow down the band gap energy.

Doping the semiconductor TiO_2 with various dopants may lead to an enhanced efficiency of photocatalytic system and achieve visible light sensitive photocatalysts. Dopants include anions, cations of transition metal ions and rare earth metal ions. Dopant content either changes the interfacial charge transfer rate, which directly influences the rate of e^-/h^+ pair recombination, or reduces the space-charge region of doped photocatalyst. However, the concentration of dopant needs to be optimised to a certain level to avoid the creation of new recombination centers (Irie et al., 2003). To induce visible light activated TiO_2, nonmetallic anions are utilised to substitute oxygen in TiO_2 in order to narrow the band gap. Consequently, in recent years, N-doped TiO_2 has been the most extensively studied, and achieved considerable successes in enhancing the visible-light photocatalytic (Vaiano et al., 2016b), N-doped TiO_2 has been proven to be a more promising photocatalyst material under visible irradiation for the degradation of organic pollutants compared to others, i.e. dyes with nearby 90 % degradation efficiency (Xu et al., 2007), phenol with reached 59 - 65 % degradation (Vaiano et al., 2016a). The N–TiO_2 with rice grain-like nanostructure morphology prepared by the

Paper Received: 14 March 2018; Revised: 26 July 2018; Accepted: 02 October 2018

Please cite this article as: Nguyen D.T., Ho T.N.S., Le M.V., 2019, Removal of β-naphthol in water via photocatalytic degradation over n-tio 2 /sio 2 nanocomposite under simulated solar light irradiation, Chemical Engineering Transactions, 72, 1-6 DOI:10.3303/CET1972001

electrospinning method, showed superior Methylene Blue degradation compared to TiO_2 rice grains (Babu et al., 2012). Vaiano et al. (2016b) explained that the substitution of N for O in the anatase TiO_2 crystal would yield a band-gap narrowing driven by mixing of N 2p states with O 2p states because their energies are very close, and thus the band gap of N-TiO_2 is narrowed and able to absorb visible light.
Besides narrowing the bandgap energy, a large surface also plays a vital role in photocatalytic reaction efficiencies (Guo et al., 2014). It can provide a large amount of active sites, and absorb more target molecules in order to promote the photo-induced reaction rates. Silica, one of the best adsorbent candidates, has been used in composition of TiO_2/SiO_2. Not only does a porous structure of silica offer high surface area, bio-chemical inertia but also it enables to control effectively the growth of TiO_2 particles leading to smaller size, larger specific surface area and increase the overall photocatalytic activity (Kibombo et al., 2011). It is suitable to combine silica with TiO_2 to treat organic pollutants in the waste water. To the best of our knowledge, there are only few studies regarding the photocatalytic activity of TiO_2/SiO_2 composite material for degradation of β-naphthol under simulated solar irradiation.
The objective of this study is to develop an effective N-TiO_2/SiO_2 photocatalyst materials which is studying the effect of Si:Ti molar ratio, of nitrogen dopant concentration on the photocatalytic activities of materials. The photocatalyst degradation rates of β-naphthol over photocatalyst powder was evaluated with varying concentrations of SiO_2, concentrations of nitrogen dopant, calcined temperature under simulated solar irradiation.

2. Experimental

2.1 Materials and reagents

All reagents were used as received without further purification. The titanium n-butoxide (TNB) (98 %) as a titania source was purchased from Across, β-naphthol (99 %), acetylacetone (98 %) and poly ethylene glycol (PEG, 98 %) were supplied by Sigma-Aldrich. Tetraethyl orthosilicate (TEOS, 99 %) as a silicon source was purchased from Merck. Urea (> 99 %) was supplied by Fisher Chemical.

2.2 Preparation of TiO_2/SiO_2 samples

First, SiO_2 solution was obtained from a mixture of EtOH, acid nitric, double distilled water and TEOs in volume ratios of EtOH:HNO_3:H_2O:TEOs to be 3.5 : 1.0 : 0.5 and stirred at room temperature for 1 h. Whereas, TiO_2 solution was prepared by mixing TNB, EtOH and AcAc in the volume ratio of 4 : 11 : 1. The TiO_2 solution was added dropwise into the SiO_2 solution and keep stirring for 30 min at 25 °C. Then, the mixture was heated to 75 °C under continuous stirring for 90 min before aged at room temperature for 24 h. Subsequently, the gel was dried at 120 °C for 30 min before undergoing calcining at 450, 550 and 650 °C for 2 h, which were named as TS450, TS550 and TS650.
As for the N-doped TiO_2/SiO_2 samples, solutions were obtained in the same manner to TiO_2/SiO_2 solutions in which, an approximate amount of urea was dissolved into TiO_2/SiO_2 solutions. Finally, the gel was then dried and calcined at 550 °C for 2 h. The samples were named according to the molar ratio of nitrogen and titania of 5 / 95, 10 / 90, 20 / 80 and 30 / 70 followed by N05TS, N10TS, N20TS and N30TS.

2.3 Characterisation

The phase compositions and crystal structures of the samples were determined by X-ray diffraction (XRD) using a D2 Phaser (Bruker, USA) with Cu Kα_ radiation (λ = 0.154 nm). Images of samples' morphology were taken by Scanning Electron Microscope (SEM) using JSM-6500F, JEOL. The band-gap energy of each sample was calculated from diffuse reflectance spectra (DRS) ranging from 850 to 220 nm, scanning step of 2 nm, at the rate of 400 nm/min using a Solid UV-vis JASCO V-550 equipment. Specific surface area Brunauer–Emmett–Teller (BET) was obtained by nitrogen adsorption – desorption isotherms at 77.3 K on Quantachrome Instruments version 11.0. The calculated crystallite size was determined by the Scherrer Eq(1) at (101) peak. In which β is the full width at half-maximum of the diffraction peak (FWHM), k = 0.9 is a shape constant, D is the crystallite size and θ is the Bragg angle.

$$D = \frac{k.\lambda}{\beta.\cos\theta} \quad (1)$$

2.4 Photodegradation experiments

β-naphthol solution with initial concentration of 10 ppm and natural pH of 6 was employed as the target to evaluate the photocatalytic activity of the samples under the irradiation of simulated visible light using a 25 W lamp (Natural light PT 2191-ExoTerra) with wavelength region from 390 to 640 nm, in which the most intense wavelength is located at 540 nm. The lamp was placed above the reactor. In a typical, the process of

degradation was performed in a photoreactor where 0.20 g catalyst was suspended in 200 mL of 10 ppm β-naphthol solution. During the photocatalytic process, the solution was stirred constantly and the temperature in photoreactor was maintained at 30 ± 2 °C using a water cooling jacket. The mixture was stirred in the dark for 120 min with the purpose of ensuring adsorption–desorption equilibrium before conducting the visible light irradiation. After each interval 30 min, the aliquots were withdrawn using a syringe and filtered through a 0.45 μm Nylon syringe filter for subsequent β-naphthol concentration analysis. The remaining β-naphthol concentration was then determined by a Hitachi UV-Vis spectrophotometers equipped with an Optics ISS-UV/VIS light source with a wavelength range of 200-400 nm. Degradation of the β-naphthol was tracked by its absorption peak at 223 nm. To evaluate the catalytic reusability, the catalytic after degradation process was washed in alcohol and heat treated at 250 °C for 2 h to remove totally β-naphthol contaminant.

3. Result and discussion

3.1 Catalyst characterisation

Powder X-ray diffraction patterns powder calcined at various temperatures are shown in Figure 1a. It is revealed that all samples had the pure anatase phase with the identical peaks at 2θ diffraction angles of 25.2° (101), 36.9° (004), 48.24° (200), 54.86° (211) and 63.01° (204) which are well-indexed with the JCPDS card No 21-1272. No diffraction peaks representing SiO_2 phase are detected in any samples, which indicates that SiO_2 amorphous phase is stabilised in the composite. It is known that the transformation of anatase to rutile phase takes place at temperatures from 600 to 700 °C (Alzamani et al., 2013). However, in this study, the single phase of anatase still remained as the temperature reached 650 °C and without any peak of rutile phase, this is due to the formation of the Ti-O-Si linkage which inhibited the phase transformation at high temperature (Mahyar et al., 2010). In addition, the diffraction peaks become slightly sharper and higher with increasing calcined temperature. The crystallite size of anatase TiO2 increased from 6.33 to 7.01 to 11.17 nm when the calcination temperature went up from 450 to 550 to 650 °C, which is consistent with the literature (Zhang et al., 2009). Figure 1b shows the XRD patterns of all 550 °C calcined nitrogen-doped TS composite photocatalysts with different N/Ti molar ratio with anatase phases. It is noticeable that nitrogen-doping sample exhibits typical structure of TiO_2 crystal without any detectable dopant related peaks which means that nitrogen-doping does not change its crystal structure. The reason can be due to the fact that the nitrogen species have moved into either the interstitial positions or the substitutional sites of the TiO2 crystal structure. The intensity of TiO2 peak of doping samples tend to become higher and stronger, this might originate from the compressive strains caused by the different bonding characteristics of O and N (Wu et al., 2014).

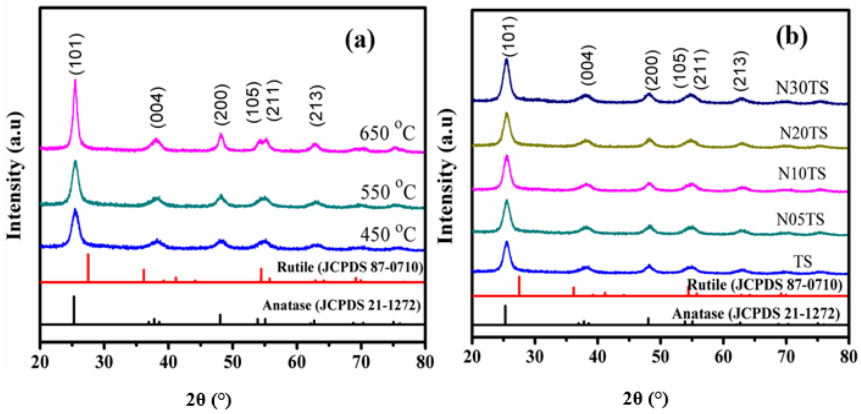

Figure 1: XRD pattern of (a) various calcined temperature TiO_2/SiO_2 powder and (b) 550 °C calcined N- doped TiO_2/SiO_2 powder

The average crystallite size of the prepared particles is given in Table 1. Crystallite size of TiO_2/SiO_2 composite oxides is smaller than that of the pure TiO_2 (P25). This phenomenon is attributed to the formation of Si-O networks by excessive SiO_2, which prevents the production of anatase crystallites (Shifu and Gengyu, 2006). It is noticeable that the crystallite size of the anatase phase decrease with increases of nitrogen doping because of the effect of nitrogen content in the composite. It was found that TiO_2/SiO_2 doped with 30 mol% of nitrogen (N30TS) shows the smallest crystallite size.

Table 1: Crystallite size of 550 °C calcined TiO_2-SiO_2 composite

Sample	Average crystallite size (nm)
P25	21 (Raj and Viswanathan, 2009)
TS	7.01
N05TS	6.81
N10TS	6.96
N20TS	6.79
N30TS	6.75

Figure 2 shows the EDX spectrum of N30TS sample. Table 2 shows the EDX analysis of N30TS. The signals of Ti and O on the spectrum are caused by TiO_2. The detected Si signal confirms the existence of SiO_2 in the sample and the atom fraction of Si/(Ti+ Si) was measured to be 15.23 % that is close to the initial value of 15 %. The atom fraction of N/Ti is measured to be 29.8 / 70.2, which is nearly consistence with the initial ratio of 30 / 70.

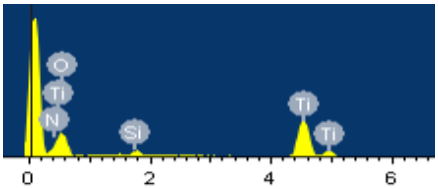

Figure 2: EDX spectra of N30TS

Table 2: The EDX analysis of N30TS

Element	Weight (%)	Atom (%)
N	4.47	7.12
O	55.05	73.45
Si	3.92	2.96
Ti	36.29	16.47
Total	100	100

The Kubelka–Munk function (Spadavecchia et al., 2010) was used to calculate the band gap energy of different samples by plotting $[F(R) - hv]^{1/2}$ with the energy of light (hv). The band gap energies are shown in Figure 3, revealing that the band gap energies those of doped samples were narrowed by nitrogen doping concentration from 5 to 30 %. Doping too much N (20 or 30 %) can result in shifting to shorter wavelength, calculated of 3.00 eV for 20 % N and 3.06 eV for 30 % N-doping sample.

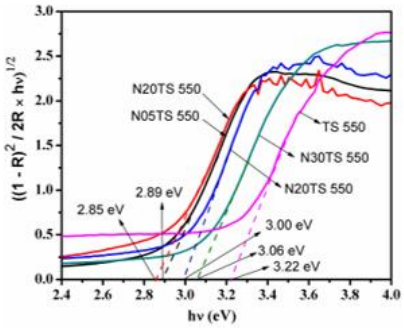

Figure 3: Kubelka–Munk modified spectra for undoped and N-doped TS550 powders

3.2 Photocatalytic activities

The photocatalytic activities of materials were studied through degradation of β-naphthol for periodical time irradiation. Generally, the dependence of β-naphthol concentration on the irradiation time can be quantitatively estimated by the kinetic of photodegradation reaction, which is described by integrated rate law equation Eq(2):

$$\ln\frac{C}{C_0} = -kt \quad (2)$$

Where, k is the apparent first-order rate constant, C and C_0 are the β-naphthol concentration at initial and after irradiation.

The photocatalytic activity of samples was evaluated by the decomposition of 10 ppm β-naphthol solution, as shown in Figure 4. The most notable feature is that all of samples with the present of SiO_2 outstripped outmatch that of P25 sample. The photocatalytic activity of TS550 catalyst showed the highest photocatalyst activities, which reached approximately 89.41 % β-naphthol degradation after 300 min irradiation and the reaction rate constant k = 0.0071 min^{-1}. Reaction rate decreased when temperature passed 650 °C as shown in Table 3. 550 °C was chosen as the optimal calcined temperature for preparing the photocatalyst.

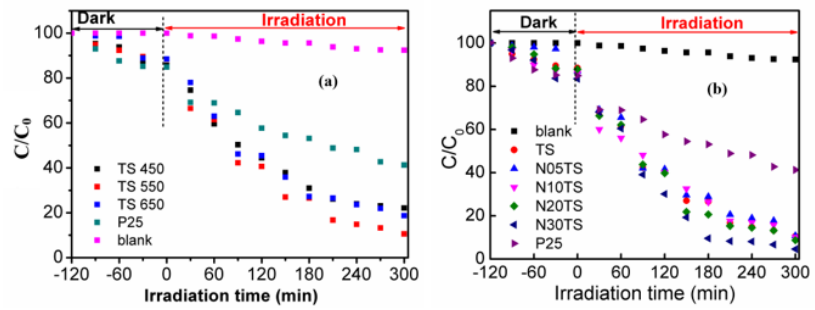

Figure 4: Photocatalytic degradation of β-naphthol over (a) various calcined temperature TiO_2-SiO_2 powder and (b) N–doped TS powder photocatalysts under simulated solar- light irradiation

As shown in Figure 4b, most N-doped samples enhanced the β-naphthol degradation efficiency compared to undoped sample (TS). Table 3 summaries the first order degradation rates of synthesised samples and P25. In the presence of a 10 % nitrogen, the photocatalytic activity of TS was obviously enhanced. The activity of TiO_2 sample was further improved with increasing percentage of nitrogen up to 30 %, reached 95.40 %. After 3 h, β-naphthol was decomposed about 90 to 95 % over N-doped samples. The most striking point is that the specific surface area of N30TS catalyst was far larger than that of undoped sample at the same condition, which were 98.23 m^2/g and 79.633 m^2/g. The larger surface area can effectively adsorb pollutants onto the reactive sites of the catalysts, thus improves the activity in degradation of β-naphthol (Zhang et al., 2016).

Table 3: The photo-activity efficiency and the first reaction rate constants for various samples

Sample	The degradation yield (%)	The first reaction rate constants, k (min^{-1})	R^2
P25	58.75	0.0025	0.97
TS450	77.90	0.0052	0.98
TS550	89.41	0.0071	0.99
TS650	81.32	0.0055	0.99
N5TS	89.25	0.0069	0.99
N10TS	89.89	0.0069	0.99
N20TS	91.25	0.0076	0.98
N30TS	95.40	0.0099	0.99

4. Conclusions

TiO_2/SiO_2 composite and N-doped TiO_2/SiO_2 samples were successfully synthesised in the single anatase phase. N-doped TiO_2/SiO_2 samples enhance the solar light responsive in photocatalytic degradation of β-naphthol. The N–doped TiO_2/SiO_2 samples which were calcined at 550 °C with molar ratio of TiO_2/SiO_2 of 85/15 represented the high degradation efficiency, from 89.41 % to 95.4 %, which was higher than that of P25 (58.75 %). This study initially revealed that the N-doped TiO_2/SiO_2 nanocomposite is a promising photocatalyst material in wastewater treatment under solar-light irradiation.

Acknowledgments

This research is funded by Vietnam National University Ho Chi Minh City (VNU-HCM) under grant number 562-2018-20-02.

References

Alzamani M., Shokuhfar A., Eghdam E., Mastal S., 2013, Study of annealing temperature variation on the structural properties of dip-coated TiO_2-SiO_2 nanostructured films, Iranian Journal of Materials Science and Engineering, 10, 39-45.

Babu V.J., Kumar M.K, Nari A.S, Kheng T.L, Alakhverdiev S.I, Ramakrishna S., 2012, Visible light photocatalytic water splitting for hydrogen production from N-TiO_2 rice grain shaped electrospun nanostructures, International Journal of Hydrogen Energy, 37, 8897-8904.

Guo N., Liang Y., Lan S., Liu L., Ji G., Gan S., Zou H., Xu X., 2014, Uniform TiO_2–SiO_2 hollow nano spheres: synthesis, characterization and enhanced adsorption–photodegradation of azo dyes and phenol, Applied Surface Science, 305, 562-574.

Hu M., Cao Y., Li Z., Yang S., Xing Z., 2017, Ti^{3+} self-doped mesoporous black TiO_2/SiO_2 nanocomposite as remarkable visible light photocatalyst, Applied Surface Science, 426, 734-744.

Irie H., Watanabe Y., Hashimoto K., 2003, Nitrogen-concentration dependence on photocatalytic activity of $TiO_{2-x}N_x$ powders, The Journal of Physical Chemistry B, 107, 5483-5486.

Kumar S.G., Rao K.K., 2017, Comparison of modification strategies towards enhanced charge carrier separation and photocatalytic degradation activity of metal oxide semiconductors (TiO_2, WO_3 and ZnO), Applied Surface Science, 391, 124-148.

Kibombo H.S., Zhao D., Gonshorowski A., Budhi S., Koppang M. D., Koodali R. T., 2011, Cosolvent-induced gelation and the hydrothermal enhancement of the crystallinity of titania−silica mixed oxides for the photocatalytic remediation of organic pollutants, The Journal of Physical Chemistry C, 115, 6126-6135.

Ma T., Wu J., Mi Y., Chen Q., Ma D., Chai C., 2017, Novel Z-Scheme g-C_3N_4/C@Bi_2MoO_6 composite with enhanced visible-light photocatalytic activity for β-naphthol degradation, Separation and Purification Technology, 183, 54-65.

Makhdoomi H., Moghadam H.M., Zabihi O., 2015, Effect of different conditions on the size and quality of titanium dioxide nanoparticles synthesized by a reflux process, Research on Chemical Intermediates, 41, 1777-1788.

Mahyar A., Behnajady M.A., Modirshahla N., 2010, Characterization and photocatalytic activity of SiO_2-TiO_2 mixed oxide nanoparticles prepared by sol-gel method, India Journal of Chemistry, 49A, 1593-1600.

Qu X., Alvarez P.J., Li Q., 2013, Applications of nanotechnology in water and wastewater treatment, Water research, 47, 3931-3946.

Raj K., Viswanathan B., 2009, Effect of surface area, pore volume and particle size of P25 titania on the phase transformation of anatase to rutile, Indian Journal of Chemistry, 48,13978-13982.

Shifu C., Gengyu C., 2006, The effect of different preparation conditions on the photocatalytic activity of TiO_2·SiO_2/beads, Surface and Coatings Technology, 200, 3637-3643.

Spadavecchia F., Cappelletti G., Ardizzonea S., Bianchi L.C.,Cappelli S., Olivaa S., Scardi P., Leoni M., Fermoc P., 2010, Solar photoactivity of nano-N-TiO_2 from tertiary amine: role of defects and paramagnetic species, Applied Catalysis B: Environmental, 96, 314-322.

Vaiano V., Sacco O., Sannino D., Ciambelli P., 2016a, N-Doped ZnO Nanoparticles Supported on ZnS based Blue Phosphors in the Photocatalytic Removal of Eriochrome Black-T Dye, Chemical Engineering Transactions, 47, 187-192.

Vaiano V., Sacco O., Sannino D., Di Capua G., Femia N. 2017, Enhanced Performances of a Photocatalytic Reactor for Wastewater Treatment Using Controlled Modulation of LEDs Light, Chemical Engineering Transaction, 57, 553-558.

Vaiano V., Sacco O., Sannino D., Stoller M., Ciambelli P., Chianese A., 2016b, Photocatalytic Removal of Phenol by Ferromagnetic N- TiO2/SiO2/Fe3O4Nanoparticles in presence of Visible Light Irradiation, Chemical Engineering Transactions, 47, 235-240.

Wu Q., Li W., Wang D., Liu S., 2014, Preparation and characterization of N-doped visible-light-responsive mesoporous TiO_2 hollow spheres, Applied Surface Science, 299, 35-40.

Xu S., Shangguan W., Yuan J., Chen M., Shi J., 2007, Preparations and photocatalytic properties of magnetically separable nitrogen-doped TiO_2 supported on nickel ferrite, Applied Catalysis B: Environmental, 71, 177-184.

Zhang M., Shi L., Yuan S., Zhao Y., Fang J., 2009, Synthesis and photocatalytic properties of highly stable and neutral TiO_2/SiO_2 hydrosol, Journal of Colloid and Interface Science, 330, 113-118.

Zhang W., Song N., Guan L.X., Li F.L., Yao M., 2016, Photocatalytic degradation of formaldehyde by nanostructured TiO_2 composite films, Journal of Experimental Nanoscience, 11, 185-196.